01 Feb 2000

Analysis of Deformation Data at Parkfield, California: Detection of a Long-Term Strain Transient

Stephen S. Gao
Missouri University of Science and Technology, sgao@mst.edu

Paul G. Silver

Alan T. Linde

Recommended Citation

S. S. Gao et al., "Analysis of Deformation Data at Parkfield, California: Detection of a Long-Term Strain Transient," *Journal of Geophysical Research Solid Earth*, vol. 105, no. B2, pp. 2955-2967, American Geophysical Union (AGU), Feb 2000.
The definitive version is available at https://doi.org/10.1029/1999JB900383

JOURNAL OF GEOPHYSICAL RESEARCH, VOL. 105, NO. B2, PAGES 2955–2967, FEBRUARY 10, 2000

Analysis of deformation data at Parkfield, California: Detection of a long-term strain transient

Stephen S. Gao,[1] Paul G. Silver, and Alan T. Linde

Department of Terrestrial Magnetism, Carnegie Institution of Washington, D. C.

Abstract. Analysis of more than a decade of high-quality data, particularly those from the two-color electronic distance meter (EDM), in the Parkfield, California, area reveals a significant transient in slip rate along the San Andreas Fault. This transient consists of an increase in fault slip rate of 3.3 ± 0.9 mm/yr during 1993.0 to 1998.0. The most reliable fault creep instruments show a comparable increase in slip rate, suggesting that the deformation is localized to the fault which breaks the surface. There was also an increase in precipitation around 1993. It is unlikely, however, that this anomaly is due directly to hydrology, as its spatial distribution is what would be expected for increased slip on the San Andreas Fault. The increase in slip rate corresponds temporally to a dramatic increase in seismicity, including the four largest earthquakes in the period 1984–1999 that occurred along a 6-km segment of the fault just to the north of the EDM network. There was also a previously reported anomaly in borehole shear strain [*Gwyther et al.*, 1996] that closely corresponds temporally to the transient in EDM data. Solely on the basis of EDM data the transient can be modeled as a slip event on a 10-km-long segment of the fault. The calculated shear strains from this model, however, are not consistent with the observed ones. A compatible model can be found if there is increased aseismic slip to the northwest in conjunction with the four earthquakes. Support for this northwestern slip is provided by a recent study of slip rate based on microearthquake activity. We speculate that this northwestern event served to load the fault to the southeast, with the stress being partially released by the observed slip.

1. Introduction

Spatial variations in slip rate along major plate boundaries such as the San Andreas Fault (SAF) have been well-established through intensive geodetic studies during the last 2 decades. These studies have played an important role in understanding the dynamics of plate boundary zones, as well as in assessing earthquake hazard. The phenomenon of transients (i.e., temporal variations) in fault slip rate has received much less attention, primarily because of the rarity (until recently) of instrumentation capable of detecting such changes. Most previous geodetic studies of transients along the San Andreas Fault system have focused on signals directly related to major earthquakes, such as postseismic deformation [e.g., *Shen et al.*, 1994; *Wyatt et al.*, 1994; *Massonnet et al.*, 1996]. There have been, however, some notable exceptions, namely, a few studies of aseismic slip unrelated to significant earthquakes. Such events possess time constants ranging from days to more than a year. One example is a 10-day event detected by *Linde et al.* [1996] and interpreted as aseismic slow slip along the San Andreas Fault system. At longer period, *Gwyther et al.* [1992] detected a multiyear transient beginning about a year before the 1989 Loma Prieta earthquake, using data from a single borehole tensor strainmeter. On the basis of data from two such instruments, *Gwyther et al.* [1996] proposed that a shear strain anomaly occurred in the Parkfield area during 1993–1994. Because that study was based on only two sites from a single instrument type and because such a multiyear transient is at the long-period end of the band where borehole instruments are typically used, the existence of the shear strain anomaly proposed by *Gwyther et al.* [1996] has become an issue of debate. This, in turn, has motivated a more intense examination of the Parkfield deformation data set, including data that are more appropriate for studying multiyear transients. Here we examine the possibility of a temporal variation in slip rate using data from the two-color laser electronic distance meter (EDM) for the past 15 years, as well as other data sets.

[1]Now at Department of Geology, Kansas State University, Manhattan.

Paper number 1999JB900383.
0148-0227/00/1999JB900383$09.00

This systematic analysis reveals the existence of a strain transient that is best characterized by variation in fault slip rate along the San Andreas Fault. There was a significant increase in slip rate between 1993.0 and 1998.0, possibly preceded by a reduction in the slip rate from 1991.0 to 1993.0. The 1993–1994 strain anomaly proposed by *Gwyther et al.* [1996], based on tensor strain data, is likely related to the slip rate increase. Such long-term variations in slip rate are important, since they signal either a change in the driving stress, frictional resistance on the fault, or both. Possible sources of temporal variations include local stress redistribution due to nearby events, the local response to distant effects such as subtle changes in plate motion [e.g., *Press and Allen*, 1995; *Romanowicz*, 1993], viscoelastic relaxation from distant earthquakes [*Pollitz and Sacks*, 1995; *Pollitz et al.*, 1998], or environmentally induced variations in frictional resistance to slip through pore pressure variations in the fault zone.

2. Data

Several types of data recorded in the Parkfield area are systematically analyzed, including data from EDM, fault creep, borehole tensor and dilatational strain, local seismicity, and water level, as well as daily precipitation (Figure 1). Our analysis, as well as the known instrument characteristics of various strain measuring techniques, show that the EDM data are most effective in detecting multiyear transients. The EDM network at Parkfield consists of a central monument and more than a dozen reflectors (Figure 2). The distances from the central monument to a network of reflectors are measured several times each week with a two-color laser distance-measuring device. This technique is capable of resolving length changes of about 1 mm over the 1- to 9-km-long baselines [*Bakun and Lindh*, 1985; *Burford and Slater*, 1985; *Langbein et al.*, 1990, 1995; *Langbein and Johnson*, 1997]. The use of two laser beams reduces the influence of atmospheric variations.

Sixteen baselines are used in the study (Figure 2). The observations of distance change contain noise from three sources: (1) short-term instrument instability, (2) localized movement at the remote reflector sites, and (3) localized movement of the central monument at CARR. Concerning the first noise source, the standard deviation of each measurement is estimated from individual measurements during a period of several minutes. This is a relatively small source of error for multiyear time periods when slopes are being estimated. Noise from the other two sources is dominated by random walk noise (see below) and is the most significant source of error.

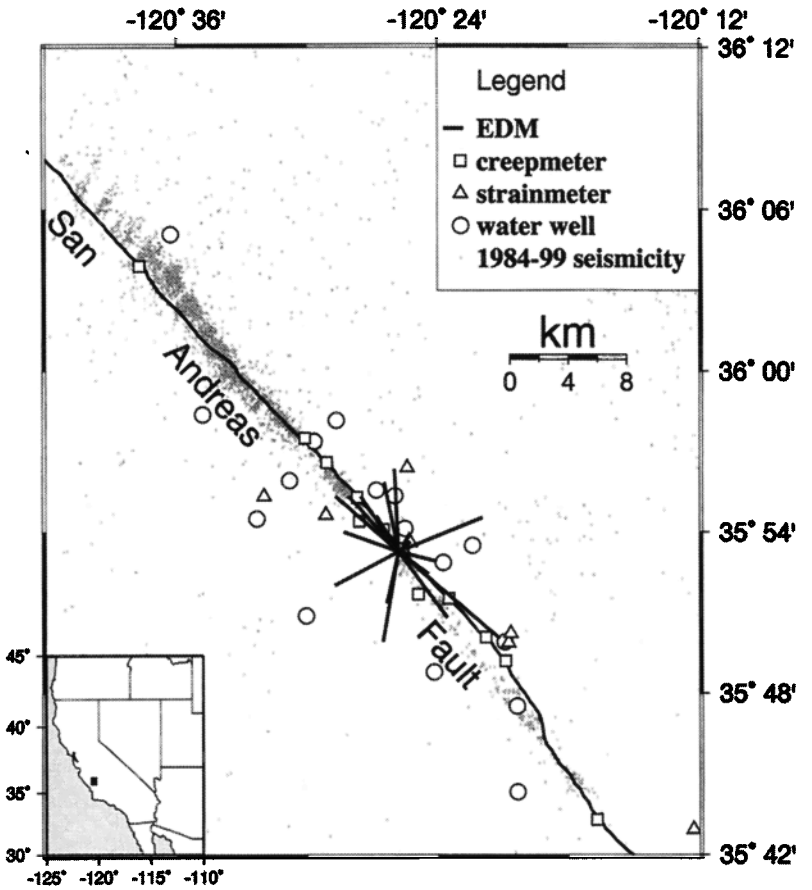

Figure 1. Locations of deformation-measuring instruments and seismicity in the Parkfield area. Shaded dots are epicenters of earthquakes for the time period of 1984.0–1999.2

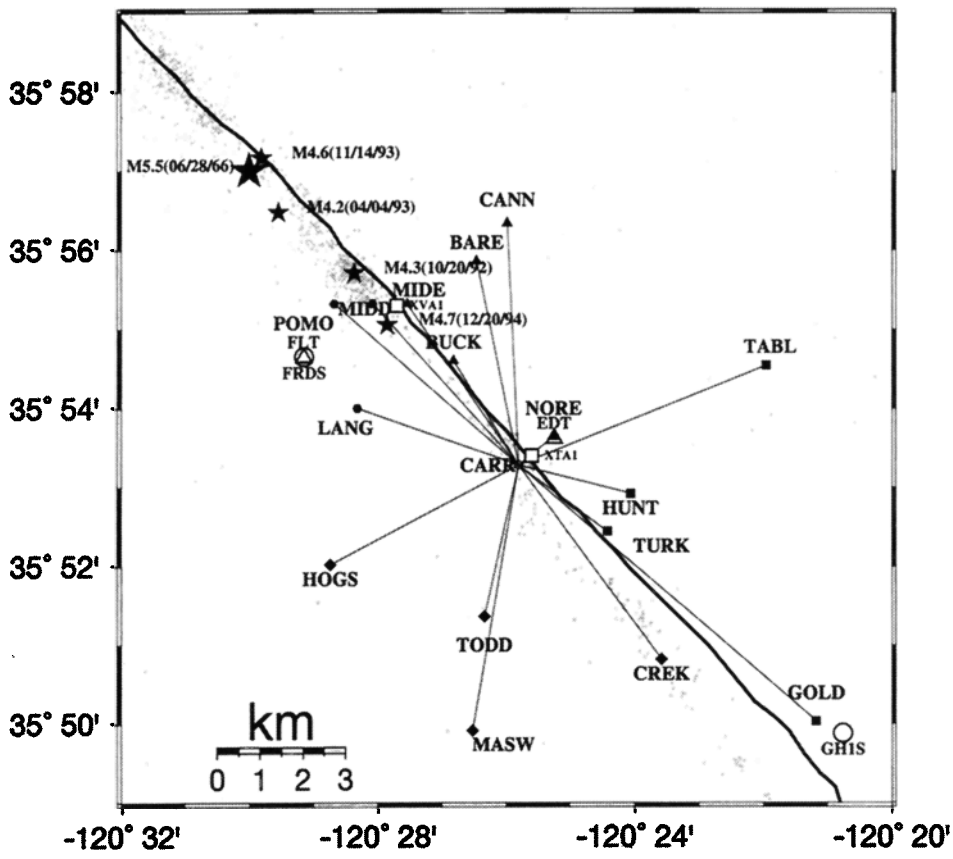

Figure 2. The electronic distance meter (EDM) network and other strain-measuring instruments used in the study. The central monument of the EDM network is located at Carr Hill (CARR), which is on the west side of the San Andreas Fault (SAF) and has a geographic coordinate of N35.888° and W120.430°. The 16 baselines used in the study between the reflectors and the central monument are divided into four groups according to their spatial relationship to the SAF. Monuments represented by solid triangles are located in the north quadrant; those represented by solid squares are in the east quadrant; diamonds are in the south; and hexagons are in the west quadrant. Also shown are two borehole dilatometers (FRDS and GH1S, circles), two borehole tensor strainmeters (FLT and EDT, open triangles), and two creepmeters (XVA1 and XTA1, open squares). Small dots are epicenters of earthquakes for the time period of 1984.0–1999.2. Small stars denote the four large earthquakes that occurred between the end of 1992 and end of 1994. Large star denotes the 1966 Parkfield earthquake.

Remote reflector noise is uncorrelated among baselines and therefore can be recognized when all baselines are used, assuming that there is a coherent component to the deformation. The third source of error, that is, the movement of the central monument at CARR, is the most serious source of error for our study. For fault-crossing baselines, length changes resulting from fault-parallel movement of CARR cannot be distinguished from rigid block motion on the other side of the fault. This is not true, however, for stations on the same side of the fault, and this fact, in principle, provides a means of separating the two effects. The distance errors $\eta(t)$ for individual baselines are a combination of temporally independent Gaussian noise $\alpha(t)$ and temporally correlated random walk noise $\beta(t)$ [e.g., *Johnson and Agnew*, 1995], that is, $\eta(t) = \alpha(t) + \beta(t)$. The random walk noise at time t is given by $\beta(t) = \sigma_r\sqrt{t}$, where σ_r is the random walk noise standard deviation for a reference time interval, customarily taken to be 1 year. Random walk noise appears to dominate for the multiyear time periods that we are interested in [*Johnson and Agnew*, 1995].

For illustration the 16 baselines used in the study are divided into four groups according to their spatial relationship with the SAF (Figure 2). Because of fault slip along the SAF, baseline lengths in the northern group are expected to decrease, and those in the eastern group are expected to increase with time. The observed variations of baseline lengths are shown in Figure 3. For the fault-crossing baselines (Figure 3) the slopes of the time series, which range from near zero to about 10 mm/yr, are approximately proportional to $\cos\theta$, where θ is the angle between the SAF and the baseline. This is the expected relation for rigid block motion along a fault, because for rigid block motion along a fault with slip rate R, the observed slope $S = R\cos\theta$. For the

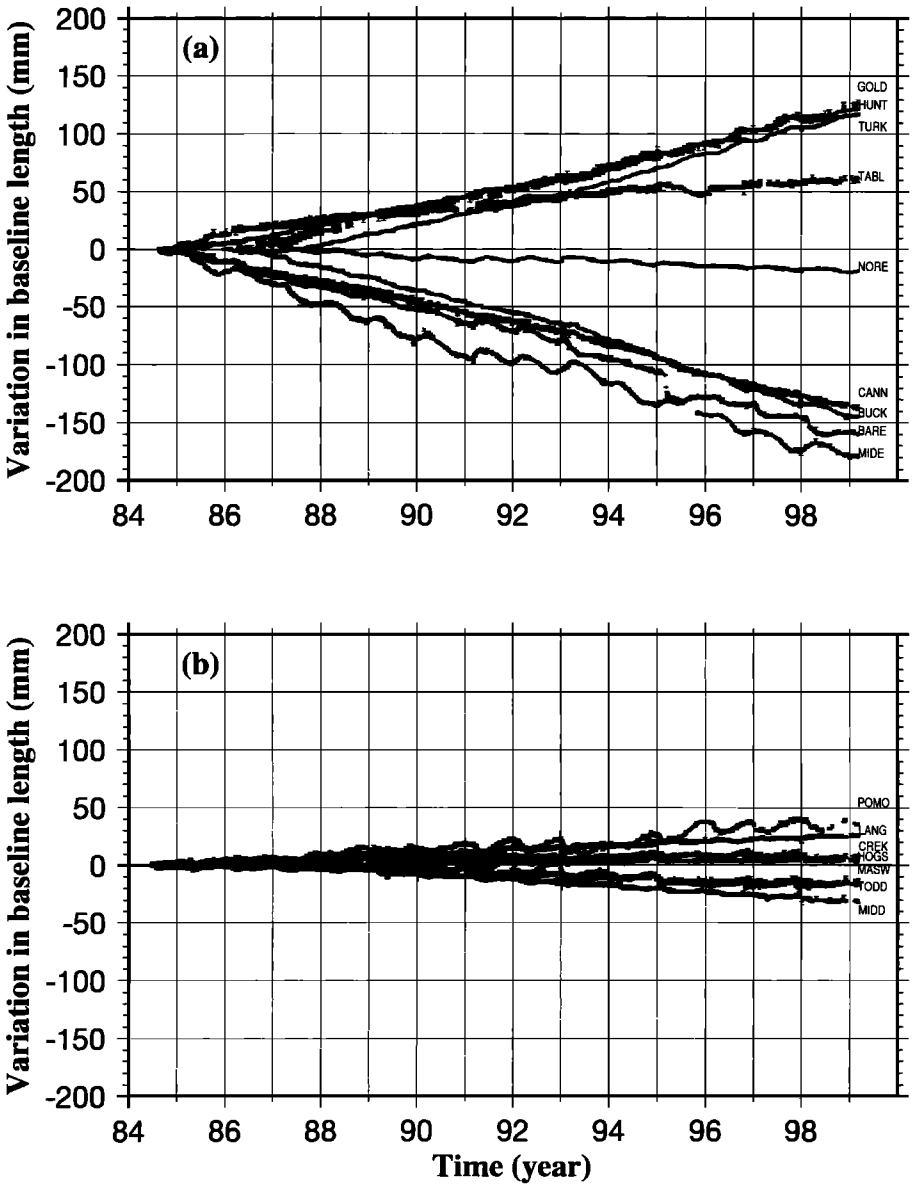

Figure 3. Time series of EDM baseline changes for the period 1984.0–1999.2. Error bars represent one standard deviation of the measurements due to white noise. The data also contain random walk noise (see text). (a) Fault-crossing baselines, (b) Baselines not crossing the fault.

non–fault-crossing baselines the slopes are small, less than 3.5 mm/yr, and are not obviously related to θ, as would be expected if the motion of the central monument were the cause. Such motions are probably the result of localized movement at the remote reflector sites or of more diffuse deformation that is not well represented by a rigid block model. The spatial patterns of baseline slope will be different from CARR motion and block fault motion. Motion of CARR will show up in all baselines and will be related to the geographic azimuth of the baseline, while block fault motion will show up in fault-crossing baselines only and will be related to the azimuth with respect to the fault trace.

Figure 4 shows detrended records that should reveal deviations from secular strain accumulation. There are several components in the residual time series. First, as is clear from Figure 4, several of the baselines, particularly BARE, MIDE, POMO, and TODD show a strong annual cycle. The annual cycle is most probably due, directly or indirectly, to precipitation. The sensitivity to precipitation varies with baseline, depending on several factors such as rock properties, topography, reflector installation conditions, and the aquifer system beneath the reflectors. The five fault-crossing baselines which are nearly parallel to the SAF (thus showing the maximum effect of fault slip) and with a low annual cycle, BUCK, CANN, HUNT, TURK, and GOLD, show systematic variations in baseline length as a function of time (Figure 4). The two baselines in the north quadrant (BUCK and CANN) have con-

cave downward shapes, while the three baselines in the east quadrant (HUNT, TURK, and GOLD) have concave upward shapes. The turning points of the curves are approximately at the beginning of 1993. Because the sense of motion in the two quadrants is opposite, the observations suggest an increase in fault slip rate after 1993.0 and perhaps a decrease before 1993.0, as discussed in Section 2.1.

2.1. Estimation of Baseline Velocities and SAF Fault Slip

We assume that the time series of a baseline can be represented as a piecewise continuous function consisting of three time periods with possibly distinct constant velocities. The three time periods, based on the characteristics of the data shown in Figure 4, are pre–1991.0, 1991.0–1993.0, and 1993.0–1998.0, with corresponding velocities $V0_i$, $V1_i$, and $V2_i$, for the ith baseline (line shortening is taken to be positive). We also allow for the presence of an annual cycle of arbitrary amplitude and phase to account for hydrologic effects. The length $d_i(t)$ of the baseline at time t is represented by

$$d_i(t) = b_i - V0_i \times (t - t_o) + \phi_i(t) + \eta_i(t) \quad (t \leq 1991.0),$$

$$d_i(t) = b_i - V0_i \times (1991.0 - t_o) - V1_i \times (t - 1991.0) + \phi_i(t) + \eta_i(t) \quad (1991.0 < t \leq 1993.0),$$

$$d_i(t) = b_i - V0_i \times (1991.0 - t_o) - V1_i \times (1993.0 - 1991.0) - V2_i \times (t - 1993.0) + \phi_i(t) + \eta_i(t) \quad (1993.0 < t \leq 1998.0),$$

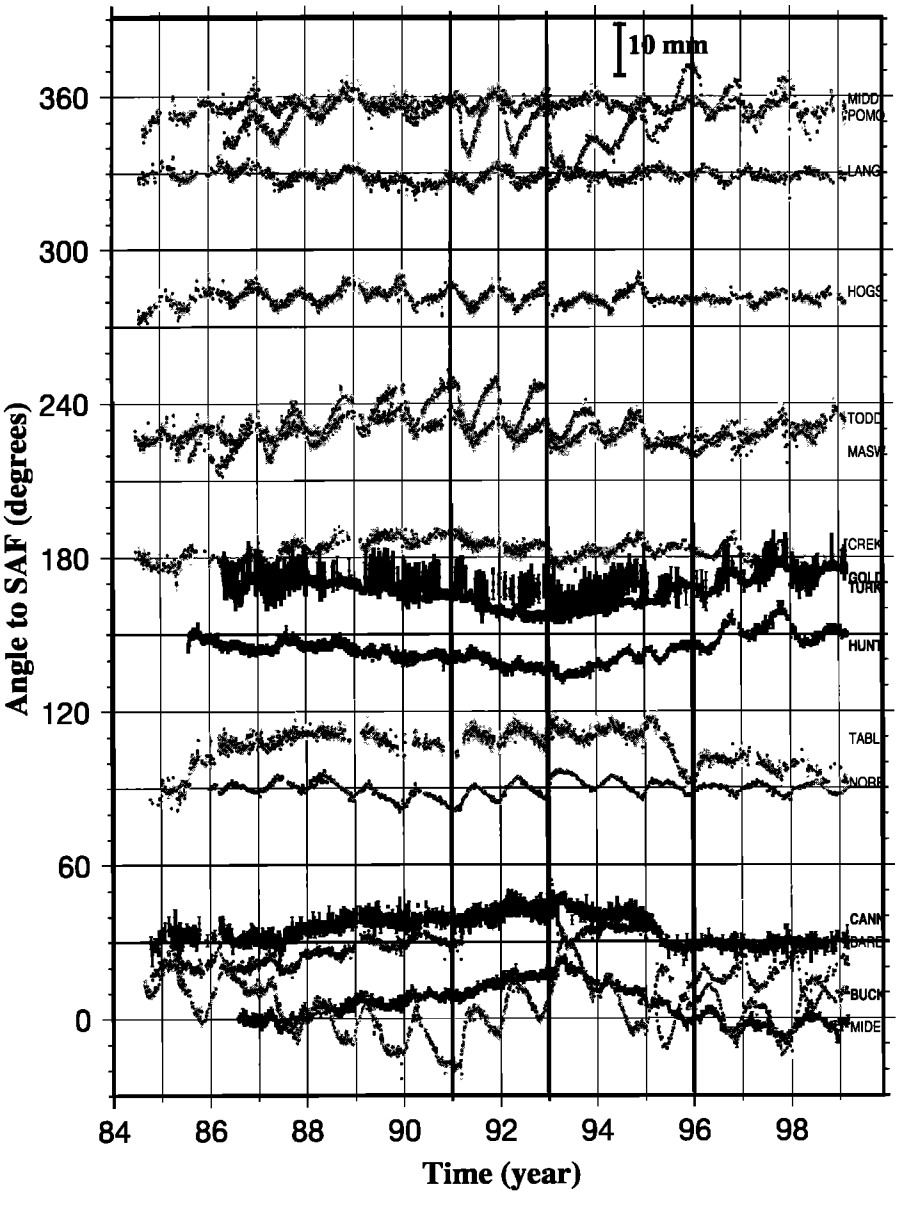

Figure 4. Linearly detrended EDM baseline changes plotted as a function of the angle the baseline makes with the SAF (clockwise from northwest). Darker lines represent fault-crossing baselines with low hydrological contamination (i.e., low annual cycles).

where b_i is the measured baseline length at the beginning for the time series t_o, $\eta_i(t)$ is measurement error, and $\phi_i(t) = A_i \sin(2\pi t) + B_i \cos(2\pi t)$. The two free parameters A_i and B_i determine the phase and amplitude of the annual cycle.

We assume that the velocities include tectonic motion and the nontectonic motion of the remote station and the central monument CARR. We will treat the nontectonic motion as a random walk–dominated error $\beta_i(t)$ and use estimates of this error provided by J. Langbein (personal communication, 1997) in the form of σ_i at a period of 1 year. We use least squares to solve for the three velocities, together with b_i, A_i, and B_i. For multiyear estimates of velocity the standard deviations in the three velocities for a random walk noise process are $\sigma_V = \sigma_i/\sqrt{T}$, where T is the time interval in years over which the particular velocity estimate is being made [*Johnson and Agnew*, 1995]. The random walk noise for the 12 remote stations with low annual cycles ranges from 0.9 to 2.9 mm/$\sqrt{T}$.

We will treat the error due to the motion of CARR two different ways: as a statistical error source and as a parameter to estimate. In the first approach we solve for an apparent fault slip velocity, which includes both the fault slip and fault-parallel CARR velocity. We concentrate on nearly fault-parallel baselines so that we can safely ignore the error due to fault-normal CARR motion. The variance in the apparent velocity estimate is calculated from both the variance of the remote site and the length of time over which the velocity is estimated. We then define the two transient velocities $\Delta V(1,2)_i = V(1,2)_i - V0_i$ with corresponding standard deviations $\sigma_{\Delta V1,2_i} = (\sigma^2_{V0_i} + \sigma^2_{V1,2_i})^{1/2}$.

Results of the fitted time series for the individual fault-crossing baselines are shown in Figure 5. As noted in Section 2, for fault slip between two rigid blocks the baseline velocities should be linear functions of $\cos\theta$. Figure 6 shows the resulting velocities ($V0_i$, $\Delta V1_i$, and $\Delta V2_i$) plotted against $\cos\theta$. The next step is to use these to estimate the corresponding SAF slip velocities, denoted as $V0$, $\Delta V1$, and $\Delta V2$. In order to account for the contribution of the motion of CARR, the uncertainty in these velocities, including CARR motion, is calculated by $(\sigma^2_{\Delta V_{1,2}} + \sigma^2_C)^{1/2}$, where σ_C is the standard deviation of fault-parallel CARR velocity, taken to be 2 mm/$\sqrt{yr}$ (J. Langbein, personal communication, 1997).

Including uncertainties in CARR and using the velocities from the five fault-crossing baselines subparallel to the fault, the corresponding SAF slip velocities are found to be $V0$ = 10.1±0.9 mm/yr, $\Delta V1$ = −1.5±1.5 mm/yr, and $\Delta V2$ = 3.3±0.9 mm/yr. These estimates correspond to reduction and increase in slip rate for 1991.0–1993.0 and 1993.0–1998.0, respectively. We find that $\Delta V2$ is significantly different from zero at the 95% level of confidence, while $\Delta V1$ is not.

In the second approach we solve explicitly for the fault-parallel and fault-normal CARR velocities $C(0,1,2)_p$ and $C(0,1,2)_n$, respectively (Table 1). As in the first approach, the resulting velocity estimate for $\Delta V2$ (3.0±0.4 mm/yr) is significantly different from zero, although $\Delta V1$ is not. For $\Delta V1$ most of the signal has been absorbed into $C1_p$. There is clearly a trade-off between these two parameters during 1991.0–1993.0. If it were possible to place an upper bound on CARR motion, in particular the differential motion between pre–1991.0 and 1991.0–1993.0, then one could further assess the significance of the signal during 1991.0–1993.0.

2.2. Other Deformation Data Sets

As noted in Section 1, there are several deformation data sets available at Parkfield that may be compared to the above results. They are either noisier, as with the creepmeter data, or less stable at multiyear period, as with the borehole strain data. It is, nevertheless, in-

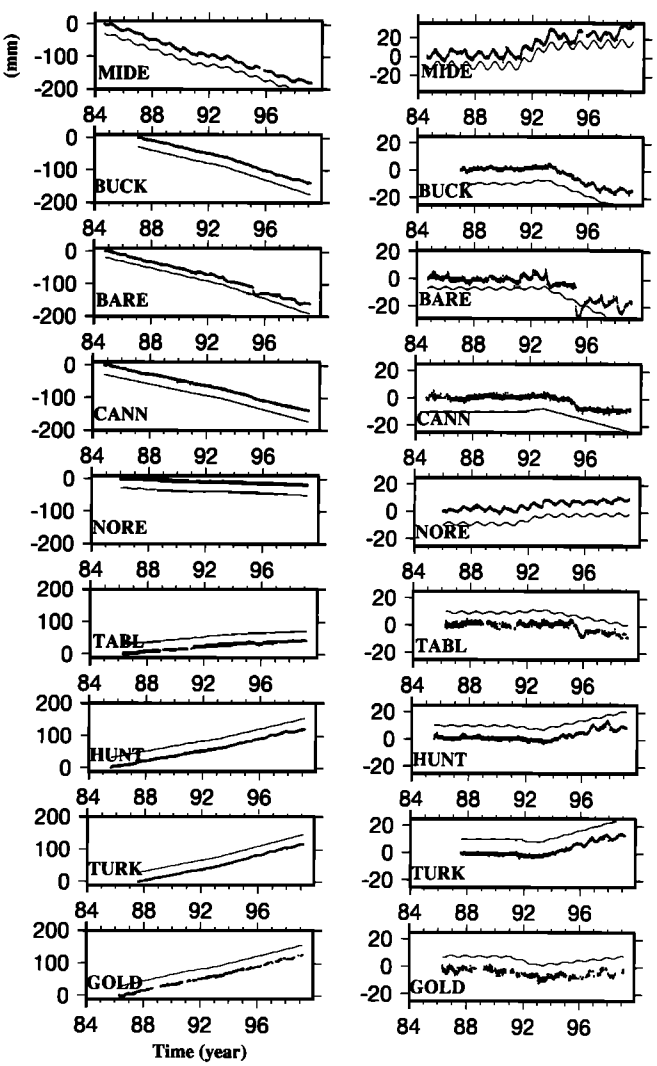

Figure 5. Observed (bold lines) and fitted (thin lines) changes in fault-crossing EDM baseline lengths. The left graphs show the original data and their fits. In the right graphs the pre-1991.0 velocity found from the inversion was removed from the baseline. The fitted and observed traces are offset for the purpose of display.

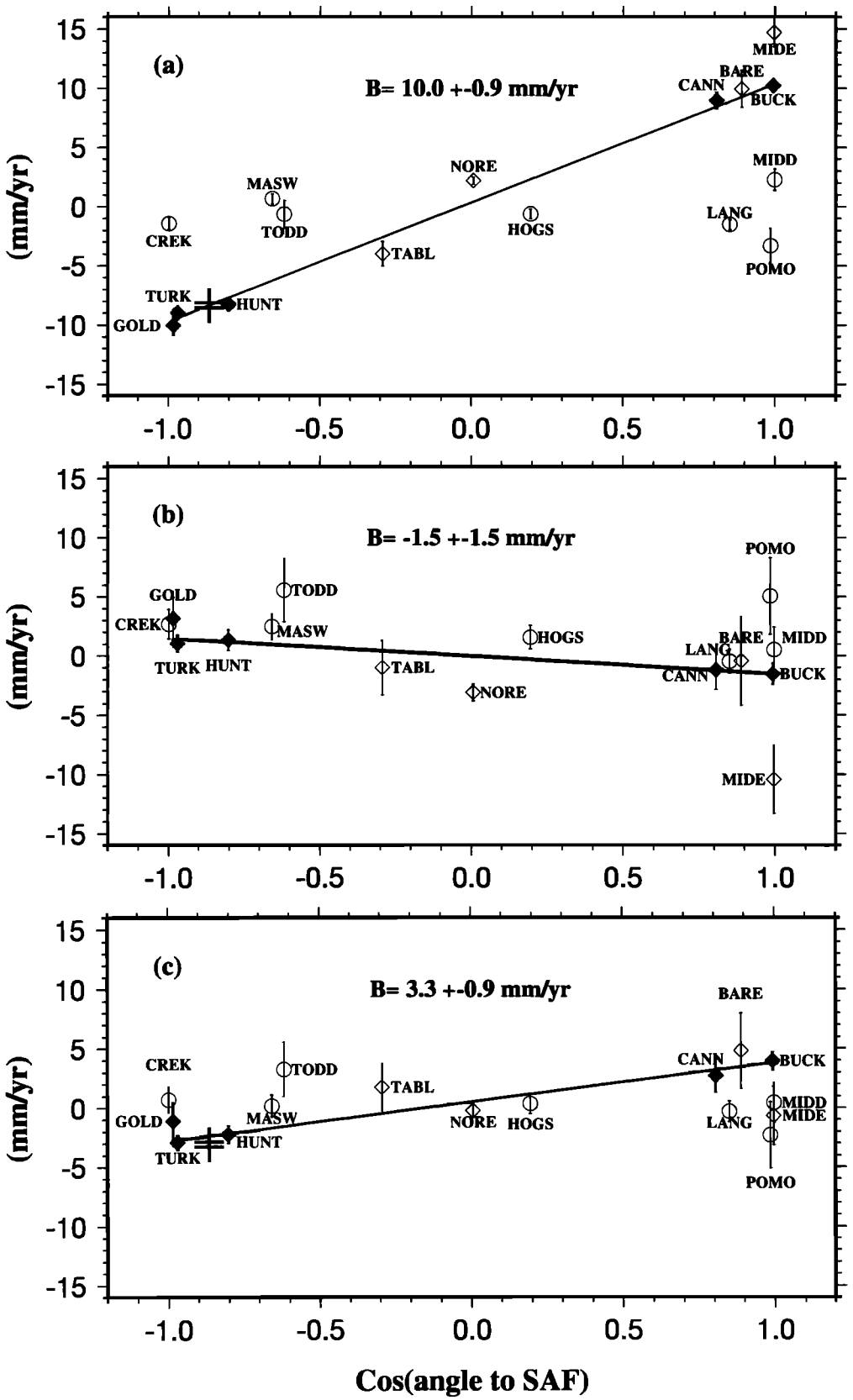

Figure 6. (a) Pre–1991.0 ($V0_i$), (b) 1991.0–1993.0 ($\Delta V1_i$), and (c) 1993.0–1998.0 ($\Delta V2_i$) baseline slopes obtained from approach 1, plotted against $\cos\theta$, where θ is the angle between the baseline and the SAF. Diamonds represent fault-crossing baselines, and circles are non–fault-crossing baselines. The fitting is based on low annual cycle fault-crossing baselines that are nearly parallel to the fault (solid diamonds, see text). Also shown (crosses in (a) and (b)) are the nearly identical velocity estimates ($V0_i$ and $\Delta V2_i$) from two creepmeters. Note good consistency with EDM data.

Table 1. Results of Inversion from Approach Two

Number	Name	Velocity, mm/yr	SD[a], mm/yr	Description
1	$V0$	10.4	0.5	pre–1991.0 velocity
2	$\Delta V1$	-0.6	0.8	1991.0–1993.0 velocity
3	$\Delta V2$	3.0	0.4	1993.0–1998.0 velocity
4	$C0_p$	0.0	0.4	CARR pre–1991.0 SAF-parallel velocity
5	$C0_n$	1.2	0.3	CARR pre–1991.0 SAF-normal velocity
6	$C1_p$	-1.7	0.6	CARR 1991.0–1993.0 SAF-parallel velocity
7	$C1_n$	-1.1	0.4	CARR 1991.0–1993.0 SAF-normal velocity
8	$C2_p$	-0.4	0.4	CARR 1993.0–1998.0 SAF-parallel velocity
9	$C2_n$	1.1	0.2	CARR 1993.0–1998.0 SAF-normal velocity

[a]Standard deviation

structive to make comparisons with these data, as they sample deformation in different ways. In order to make the most direct comparisons, we only consider stations whose locations overlap geographically with the EDM network. In addition, because of instrumental limitations, we consider only subsets of these data that are least likely to have systematic errors (Figure 2).

2.2.1. Creepmeters. Perhaps the closest in character to the EDM instruments are the creepmeters [*Schulz et al.*, 1982]. They are similar in concept to EDM except that the baselines are much shorter: 30 m versus several kilometers. Although there are no available estimates of creepmeter noise levels, which means we cannot assign uncertainties to our velocity estimates, we take the estimated secular velocity as a noise indicator. In particular, we limit ourselves to those creepmeters that recover the secular rate of approximately 10 mm/yr as inferred from the EDM data. Because creepmeters make a 30° angle with the fault, they should be seeing 87% of the full slip rate. Only two well-behaved stations yield such a rate: XVA1 and XTA1, averaging about 9 mm/yr (Figure 6). Using the same equations as for the EDM data, the estimated velocities $\Delta V2$ for both stations are approximately 3 mm/yr, nearly identical to that inferred from the EDM data (Figure 6). Taken at face value, this suggests that the creep data are detecting the same anomaly as the EDM data and furthermore that the EDM length changes are due to very localized fault slip on the San Andreas Fault that breaks the surface.

2.2.2. Strainmeters. We next consider the strain data that are contained within the EDM network (Figure 2), namely, the dilatometers [*Sacks et al.*, 1971] and three-component tensor strainmeters [*Gladwin and Hart*, 1985]. For the dilatometers, of the stations within the EDM network, VCDS, FRDS, DLDS, and GH1S were in continuous operation during the experiment; we exclude VCDS because of an extremely large annual cycle and DLDS because of a very large exponential decay [*Gwyther*, 1995]. This leaves FRDS and GH1S. Using 1989.0–1991.0 to define the exponential decay and any additional linear baseline, both stations show essentially the same signal, namely, a change in strain rate approximately at the beginning of 1993 (Figure 7). The inferred change in strain rate is 2 μ strain/yr for FRDS and 1.6 μ strain/yr for GH1S. The similarity of signals suggests that the source of strain is not localized. An infinitely long strike-slip fault, however, will have no dilatation, and it is only the end effects that could produce significant contraction. At this point we note that the timing is roughly consistent with the onset of the transient (change begins a few months before the EDM anomaly) but that the size of the signal is probably not. We will address this further in Section 3.

The other relevant borehole strain data set consists of the three-component strainmeter records used in the *Gwyther et al.* [1996] study. As noted previously,

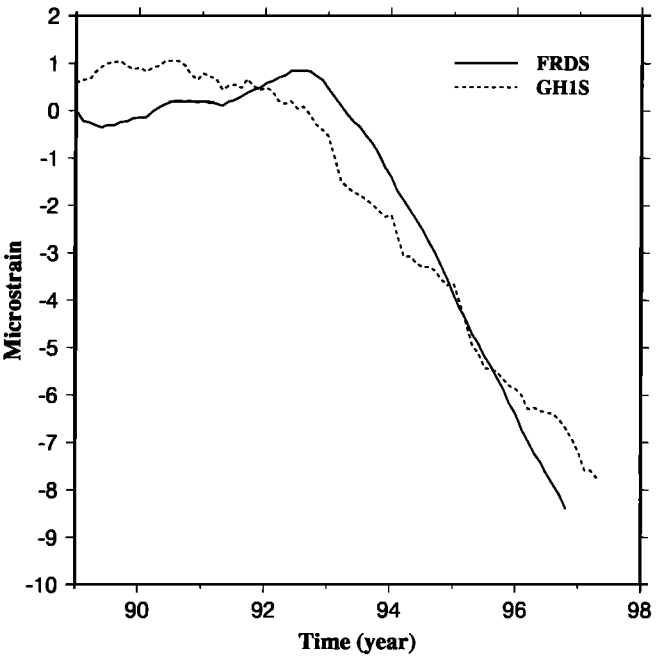

Figure 7. Detrended volumetric strain recorded by borehole dilatometers FRDS (solid line) and GH1S (dotted line). The locations of the two stations are shown on Figure 2.

these authors reported a shear-strain anomaly at stations EDT and FLT (Figure 2), beginning in 1993, that they modeled as a buried, northward and upward propagating right-lateral strike-slip source. *Gwyther et al.* focused on matching the two surface deviatoric components of the strain tensor ϵ, $\gamma_1 = \epsilon_{xx} - \epsilon_{yy}$ and $\gamma_2 = 2\epsilon_{xy}$, where x and y correspond to the east and north directions, respectively. An equivalent (and perhaps more physical) representation is in terms of the orientation Θ and size E_1 of the extensional principal strain $\mathbf{E}_1 = E_1\hat{\mathbf{e}}_1\hat{\mathbf{e}}_1$, where $E_1 = 1/2(\gamma_1^2 + \gamma_2^2)^{1/2}$ and Θ satisfies the expression $\tan(2\Theta) = \gamma_2/\gamma_1$, taking Θ to be the counterclockwise angle of the unit vector $\hat{\mathbf{e}}_1$ with respect to east. For right-lateral simple shear with the shear plane striking northwest (roughly parallel to the San Andreas Fault) $\Theta = 90°$ (north-south). The approximate values of these parameters for the two stations for 1993–1996 are $(E_1, \Theta) = (1 \times 10^{-7}/\text{yr}, -30°)$ for FLT and $(E_1, \Theta) = (3 \times 10^{-7}/\text{yr}, +30°)$ for EDT. The temporal behavior of the strain data is strikingly similar to that seen in the EDM (e.g., BUCK) data [see *Gwyther et al.*, 1996], both beginning in the first quarter of 1993, suggesting a close connection between the two data sets.

2.3. Possible Role of Precipitation/Hydrology

One possibly important source of nontectonic signal is precipitation, through its effect on subsurface hydrology. Daily and annual rainfall data obtained by averaging data from several sites in the Parkfield area are shown in Figure 8. There is a clear annual cycle with the highs being in the months from November to April and lows occurring from May to October; at multiyear periods these data reflect the end of a severe drought in 1990 or perhaps 1991, after which there was a clear increase in yearly rainfall starting from 1993, although the 1994 rainy season produced precipitation that is comparable to the pre-1990 period.

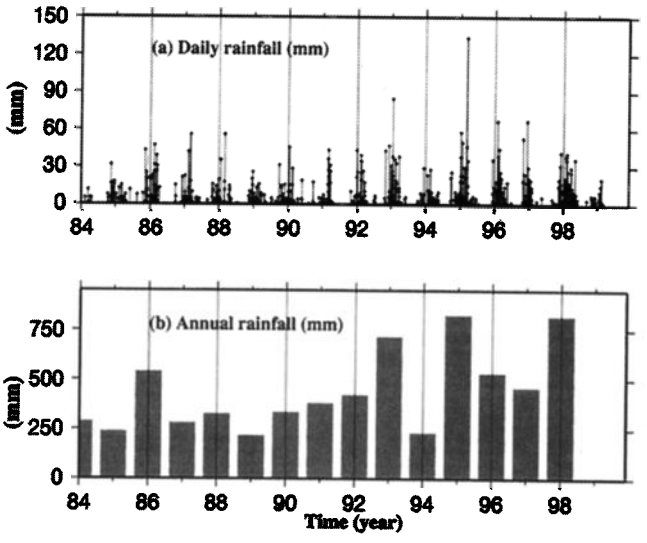

Figure 8. Daily and yearly rainfall data averaged from several sites in the Parkfield area (E. Roeloffs, personal communication, 1999). (a) Raw daily rainfall data, (b) Amount of rainfall per year. The time windows used are 1 year in length and are centered on January 1 of the years.

Since the increase in precipitation roughly coincides with the onset of the slip transient, it is natural to ask whether there is a connection between the two. Indeed, six of the eight Parkfield wells show an increase in water level, relative to pre-1993.0, which could be interpreted as the filling of subsurface aquifers by this time. The observed transient could be (1) directly due to hydrology, say, by deformation due to the filling of aquifers, (2) indirectly related, through a hydrologically induced change in fault pore pressure (and consequently frictional resistance to fault slip), or (3) simply coincidentally related to the hydrological changes.

Regarding the EDM data, the first possibility is highly unlikely, in that the spatial pattern of displacement has all of the characteristics of fault slip. Indeed, the spatial pattern of slip is nearly the same as the pattern for the secular velocity change over the last decade, which is indisputably tectonic in origin. It may be, however, that some of the data, such as the dilatometer data, have been affected directly by hydrology. It has been argued [e.g., *Gwyther et al.*, 1996] that dilatation and areal strain are more susceptible to hydrological phenomena than deviatoric strain. Concerning the other explanations, the possibility remains that increased precipitation produced a change in fault pore pressure, although there is presently no independent means of verifying this.

2.4. Transient Deformation and Seismicity

Most of the seismicity in the Parkfield region occurs along the creeping section of the SAF (Figures 1 and 2). Shown in Figure 9 is the temporal variation in seismicity for the period of 1984.0 to 1999.2 within a circle of radius 10 km centered at CARR. This zone includes most of the area covered by the instrumentation but excludes earthquakes from other areas. We used the northern California catalog archived by the University of California, Berkeley, Seismological Station. Only events with magnitude ≥ 1.3 are used to assure completeness. Whether seismicity is measured by numbers of events (Figures 9a and 9b) or by moment release (Figure 9c), there is a clear increase in seismicity after the end of 1992. During the 15-year period between 1984 and 1999, there have been only four events with magnitude of 4.2 or larger that occurred in the area, and all of them occurred between the end of 1992 and the end of 1994. As illustrated in Figure 2, these events occurred over a roughly 6-km length of fault just to the north of the EDM network and at a depth of about 9 km. As with the other data sets, the temporal correspondence suggests a connection with the observed transient.

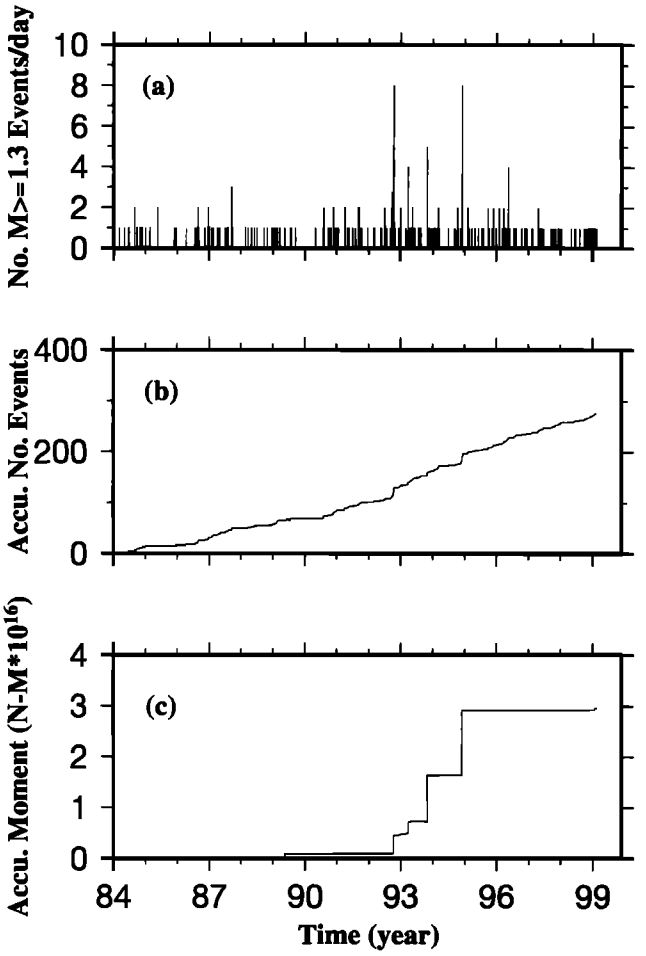

Figure 9. Temporal variations of seismicity for the period of 1984.0 to 1999.2 in a circle of radius 10 km centered on CARR. The minimum magnitude is 1.3. (a) Number of events per day, (b) Accumulated number of events, (c) Accumulated moment release. Note large increase in moment release beginning at the end of 1992.

3. Discussion

3.1. Modeling the Deformation Transient

The EDM data examined in this study are consistent with a simple model of time-variable slip along the San Andreas Fault at Parkfield. As a way of further constraining the geometry of the transient and of checking the compatibility with other data sets, we use the code of *Okada* [1992] to calculate the displacement and strain fields from dislocation sources embedded within an elastic half-space. The transient in the EDM and creep data can be modeled as a vertical right-lateral fault that extends from the surface to 9-km depth with a uniform slip of 3.3 mm/yr (Figure 10), although the depth extent is not well constrained.

With these parameters fixed, there are two additional parameters to estimate, namely, the fault length and location. The shortest fault that provides a visually acceptable fit to the EDM and creep data is 10 km long and centered 2 km southeast of CARR. A shorter fault fails to provide the large difference between fault-crossing and non–fault-crossing lines that is observed in the data.

In order to assess the compatibility with the tensor strain data, we have calculated the shear strain field for the EDM-based model. As shown in Figure 10, the predicted orientations of $\mathbf{E_1}$ actually do a poor job of matching the observed orientations for stations EDT and FLT. Indeed, the predicted and observed orientations are nearly orthogonal. The observed orientations are more consistent with the end effects from the southeastern end of a right-lateral strike-slip fault, so one way to produce the observed orientations is to limit the southeastern fault extent to no farther than CARR. This is, of course, incompatible with the EDM displacements, so that if both data sets are considered, the EDM-based model must be modified.

One way to satisfy both data sets is to add a zone of increased right-lateral slip (i.e., significantly greater than 3.3 mm/yr) farther to the northwest. This possibility is motivated by the occurrence of the four events that took place within this northwestern zone during the first 2 years of the transient (Figure 2). On the basis of their magnitude we estimate the slip on these faults to be of the order of 6 cm and fault dimension to be about 2 km. All four events occurred at about 9-km depth. We assume that there was aseismic slip accompanying these events and consider a model in which there is slow slip within adjacent regions of the fault and with overall slip comparable to that inferred from the earthquakes. In particular, we consider an event characterized by slip from 2-km to 9-km depth (above the depths of the events but not breaking the surface) and extending over a 15-km length of fault that contains the epicenters of the four events (Figure 11). We impose an accumulated slip over 5 years that is equal to 6 cm (coseismic slip) or 12 mm/yr. We note that while the coseismic displacements themselves are too small, by an order of magnitude, to account for the observed transient signals, the slow slip does give the correct orientation of $\mathbf{E_1}$ and ratio of strain magnitudes at the two tensor strain stations, although the calculated values are too small by about a factor of 2.

This model thus predicts that there should be a significant deformation transient along this northwestern segment in addition to the observed slip to the southeast. We note that while there is no relevant surface instrumentation to test this hypothesis, there is subsurface information in the form of fault zone slip rate estimates, based on the recurrence times of microearthquakes. *Nadeau and McEvilly* [1999] have recently performed such estimates in the Parkfield region, and they have, indeed, detected an increase in fault slip rate beginning in 1993. The largest increase is observed for the 10-km length of fault centered on the epicenter of the 1966 Parkfield event (Figure 2) over a depth range of about 2 to 10 km. The estimated slip rate increase is about 10 mm/yr. The center of activity subsequently

migrates to the southeast. All of this activity takes place within the northwestern fault zone defined in our model, and the inferred slip rate is similar to what we have used. Thus the simple model that we propose provides a reasonable fit to much of the deformation data collected at Parkfield.

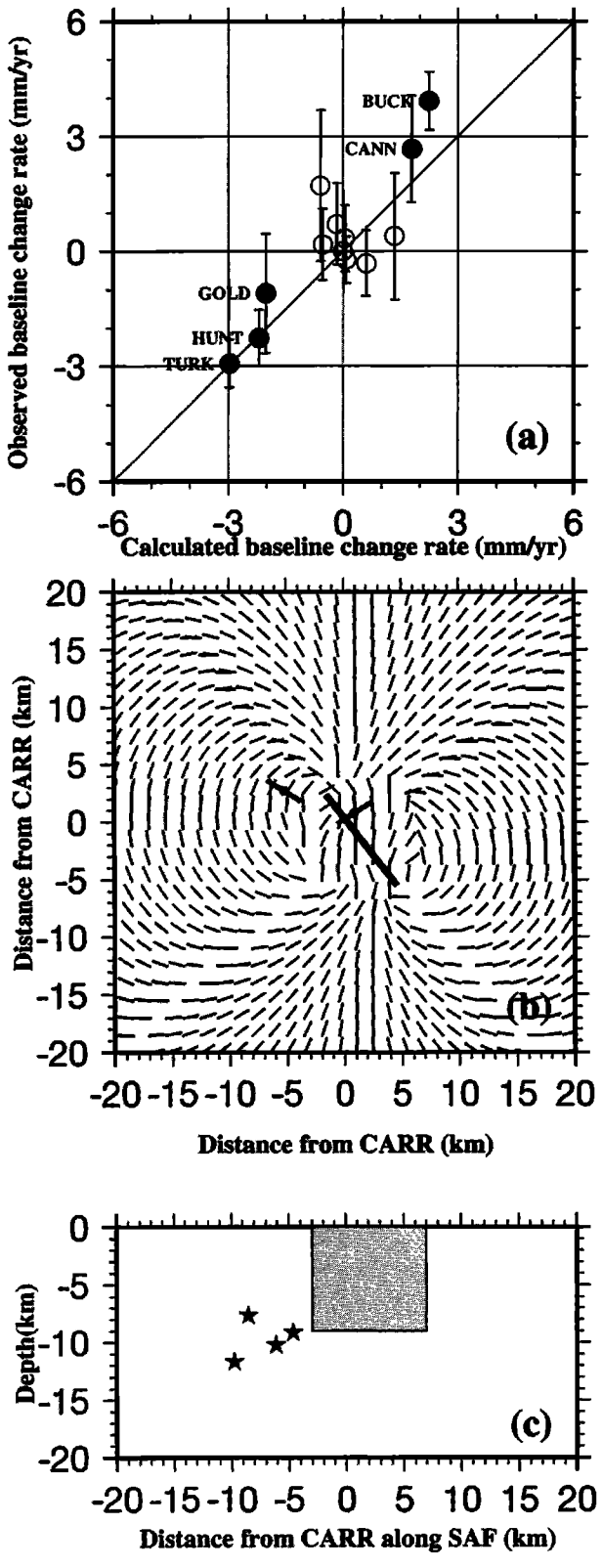

3.2. Stress Loading or Stress Release?

The existence of a transient increase in fault slip rate along the San Andreas Fault at Parkfield requires that there has been either a change in the loading stress, a reduction of frictional resistance on the fault, or both. In the first case the change in slip rate is interpreted as being due to a transient stress increase that is only partially released by the transient slip. In the second case the slip represents a transient release of stress from a reduction in frictional resistance on the fault. Is it possible to tell the difference between these two possibilities? We note that the signal in the EDM data is dominated by slip on the fault itself, while the main diagnostic for loading/release is actually the sense of shear strain away from the fault: either strain accumulation or strain release. Thus, in principle, the combined use of these short- and long-baseline data can be used to assess the stress/strain state of the fault related to transients. Taken at face value, the tensor strain data are more consistent with loading rather than a release of stress. We speculate that a combined event, consisting of the four seismic events, associated slow slip, and increased microearthquake activity along the northwestern segment, loaded the southeastern segment. That stress has been partially released by the observed slip transient farther southeast.

4. Conclusions

We have detected a deformation transient, whose most direct manifestation is an increase in the fault slip rate along the San Andreas Fault at Parkfield. On the basis of EDM data we find an increase in slip rate of 3.3 mm/yr beginning in 1993 and continuing through 1997. This slip rate is also observed on two of the more reliable creepmeters within the EDM network, suggesting that the slip is very localized to the fault and extends to the surface. These data can be modeled by uniform slip

Figure 10. Predicted baseline changes and shear strains from a strike-slip fault model consistent with the EDM data. (a) Observed versus calculated EDM baseline change for low annual cycle baselines for transient 1993.0–1998.0. The fault length is 10 km (centered 2 km southeast of CARR which is at the center of the map) and extends from surface to 9-km depth. Strike of the fault is taken to be 38° west of north. The accumulated slip for this model is 16.5 mm (3.3 mm/yr) along the entire fault. Solid circles are low annual cycle fault-crossing baselines. Positive values correspond to a decrease in baseline length. (b) The predicted orientation of principal extensional strain $\mathbf{E}_1$ (thin bars) and the observed values at two borehole tensor strain sites (bold bars with dot) along with projection of fault onto surface (long bar). Note that this model adequately fits EDM data but does not fit the $\mathbf{E}_1$ orientation. (c) Schematic cross-section of fault model. Stars denote epicenters of the four large events projected onto the fault plane.

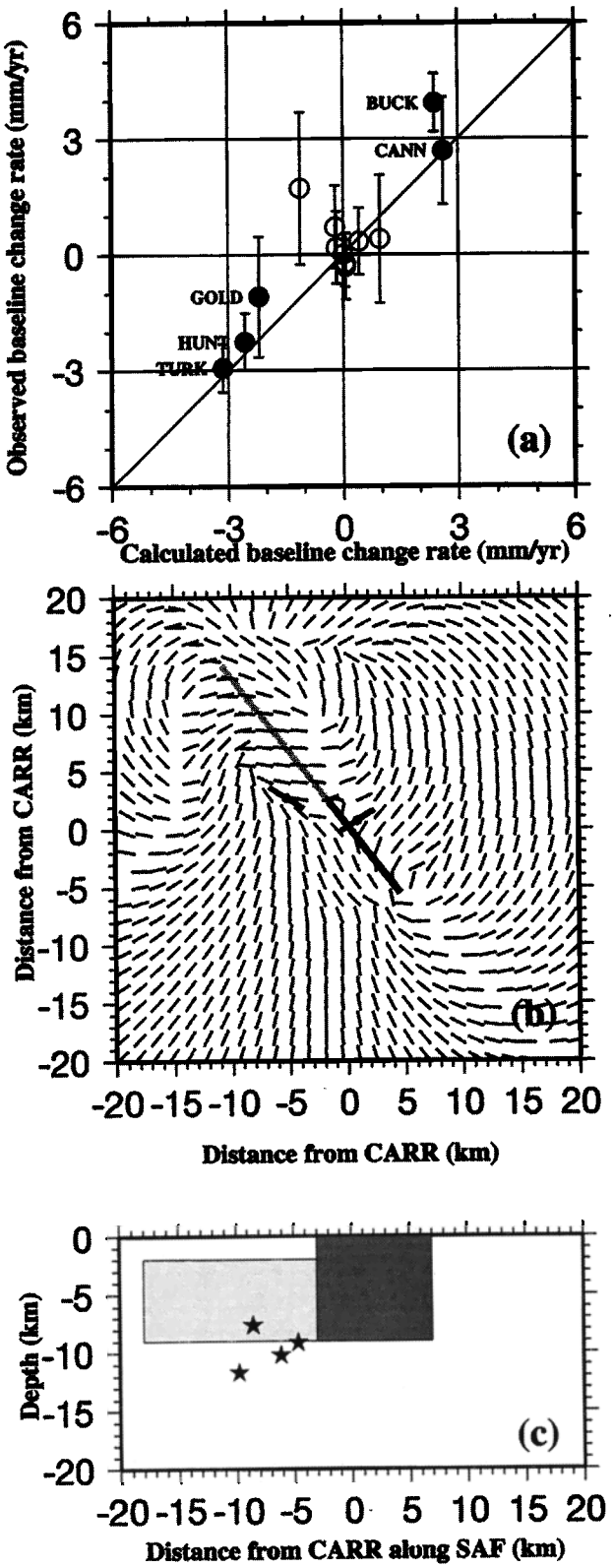

Figure 11. Same as Figure 10 but for a modified fault model with additional slip to the northwest along the region spanning the occurrence of the four $M \geq 4.2$ earthquakes. Northwestern slip is 12 mm/yr over 5 years along a patch of fault 15 km long extending from 2 to 9 km in depth (depth interval above the events). This model fits both the EDM data and the orientation of $\mathbf{E}_1$.

over a 10-km-long fault centered just south of the central EDM monument CARR. This increase in slip rate was most probably due to the loading of this segment of the fault by greater slip farther to the northwest.

Acknowledgments. Most of the data used in the study were collected by those who were involved in the Parkfield earthquake experiment. Their efforts, especially those of Malcolm Johnston, John Langbein, and Evelyn Roeloffs, in data acquisition and processing are greatly appreciated. EDM data were provided by John Langbein. Rainfall and water level data were supplied by Evelyn Roeloffs and Eddie Quilty. Seismicity was obtained from the UCB seismic station data center maintained by Doug Neuhauser. Inspiring discussions with Selwyn Sacks, Frank Press, Evelyn Roeloffs, Kelly Liu, and Sean Solomon provided us with new information and ideas. Critical reviews by Hadley Johnson, Robert King, Jim Savage, and John Langbein greatly improved the manuscript. This study was supported by NASA (NAG5-6159) and the Carnegie Institution of Washington.

References

Bakun, W. H., and A. G. Lindh, The Parkfield, California, earthquake prediction experiment, *Science, 229*, 619-624, 1985.

Burford, R. O., and L. E. Slater, Two-color laser strain monitoring in the Parkfield region, *U.S. Geol. Surv. Open File Rep., OF 85-0754*, 117-129, 1985.

Gladwin, M. T., and R. Hart, Design parameters for borehole strain instrumentation, *Pure Appl. Geophys., 123*, 59-81, 1985.

Gwyther, R. L., An investigation of aseismic fault processes in California with borehole strain measurements, Ph.D. thesis, Univ. of Queensland, Brisbane, Queensland, Australia, 1995.

Gwyther, R. L., M. T. Gladwin, and R. G. Hart, A shear-strain anomaly following the Loma Prieta earthquake, *Nature, 356*, 142-144, 1992.

Gwyther, R. L., M. T. Gladwin, M. Mee, and R. H. G. Hart, Anomalous shear strain at Parkfield during 1993–94, *Geophys. Res. Lett., 23*, 2425-2428, 1996.

Johnson, H. O., and D. C. Agnew, Monument motion and measurements of crustal velocities, *Geophys. Res. Lett., 22*, 2905-2908, 1995.

Langbein, J., and H. Johnson, Correlated errors in geodetic time series: Implications for time-dependent deformation, *J. Geophys. Res., 102*, 591-603, 1997.

Langbein, J. O., R. O. Burford, and L. E. Slater, Variations in fault slip and strain accumulation at Parkfield, California: Initial results using two-color geodimeter measurements, 1984–1988, *J. Geophys. Res., 95*, 2533-2552, 1990.

Langbein, J. O., F. Wyatt, H. Johnson, D. Hamann, and P. Zimmer, Improved stability of a deeply anchored geodetic monument for deformation monitoring, *Geophys. Res. Lett., 22*, 3533-3536, 1995.

Linde, A. T., M. T. Gladwin, M. J. S. Johnston, R. L. Gwyther, and R. G. Bilham, A slow earthquake sequence on the San Andreas Fault, *Nature, 383*, 65-68, 1996.

Massonnet, D., W. Thatcher, and H. Vadon, Detection of postseismic fault-zone collapse following the Landers earthquake, *Nature, 382*, 612-616, 1996.

Nadeau, R. M., and T. V. McEvilly, Fault slip rates at depth from recurrence intervals of repeating microearthquakes, *Science, 285*, 718-721, 1999.

Okada, Y., Internal deformation due to shear and tensile

faults in a half-space, *Bull. Seismol. Soc. Am., 82*, 1018-1040, 1992.

Pollitz, F. F., and I. S. Sacks, Consequences of stress changes following the 1891 Nobi earthquake, Japan, *Bull. Seismol. Soc. Am., 85*, 796-807, 1995.

Pollitz, F. F., R. Burgmann, and P. Segall, Joint estimation of afterslip rate and postseismic relaxation following the 1989 Loma Prieta earthquake, *J. Geophys. Res., 103*, 26,975-26,992, 1998.

Press, F., and C. Allen, Patterns of seismic release in the southern California region, *J. Geophys. Res., 100*, 6421-6430, 1995.

Romanowicz, B., Spatiotemporal patterns in the energy release of great earthquakes, *Science, 260*, 1923-1926, 1993.

Sacks, I. S., S. Suyehiro, D. W. Evertson, and Y. Yamagishi, Sacks-Evertson strainmeters, its installation in Japan and some preliminary results concerning strain steps, *Pap. Meteorol. Geophys., 22*, 159-207, 1971.

Schulz, S. S., G. M. Mavko, R. O. Burford, and W. D. Stuart, Long-term fault creep observations in central California, *J. Geophys. Res., 87*, 6977-6982, 1982.

Shen, Z., D. D. Jackson, Y. Feng, M. Cline, M. Kim, P. Fang, and Y. Bock, Postseismic deformation following the Landers earthquake, California, 28 June 1992, *Bull. Seismol. Soc. Am., 84*, 780-791, 1994.

Wyatt, F. K., D. C. Agnew, and M. Gladwin, Continuous measurements of crustal deformation for the 1992 Landers earthquake sequence, *Bull. Seismol. Soc. Am., 84*, 646-659, 1994.

S. S. Gao, Department of Geology, Kansas State University, Manhattan, KS 66506-3201. (e-mail: sgao@ksu.edu)

A. T. Linde and P. G. Silver, Department of Terrestrial Magnetism, Carnegie Institution of Washington, 5241 Broad Branch Road, NW, Washington, DC 20015. (e-mail: linde@dtm.ciw.edu; silver@dtm.ciw.edu)

(Received October 8, 1998; revised October 21, 1999; accepted October 28, 1999)